

Supplementary Information for:

Defect Control To Enhance Proton Conductivity in a Metal-Organic Framework

Jared M. Taylor^{*,†,‡}, Shun Dekura[†], Ryuichi Ikeda[†], and Hiroshi Kitagawa^{*,†,‡,#,§}

[†] Division of Chemistry, Graduate School of Science, Kyoto University, Kitashirakawa-Oiwakecho, Sakyo-ku, Kyoto 606-8502, Japan.

[‡] JST CREST, 7, Gobancho, Chiyoda-ku, Tokyo 102-0076, Japan.

[#] INAMORI Frontier Research Center, Kyushu University, Motoooka 744, Nishi-ku, Fukuoka 819-0395, Japan.

[§] Institute for Integrated Cell-Material Sciences (iCeMS), Kyoto University, Yoshida, Sakyo-ku, Kyoto 606-8501, Japan.

Synthesis. All chemicals were purchased from commercial suppliers (Aldrich, Wako, Kishida Chemicals) and were used without any further purification. The UiO-66 samples were synthesised using two methods, which were modifications of previously reported synthetic procedures.^{1,2}

The synthetic procedure involved the formation of defect-containing UiO-66 by controlling the ZrCl₄: terephthalic acid: H₂O stoichiometry during the synthesis, or by the addition of a monocarboxylic acid additive. The amounts used for samples **1** – **6** are listed in table S1. In a typical synthesis, DMF was added to a mixture of the ZrCl₄ and carboxylic acid additive and sonicated to dissolve, forming a slightly cloudy colourless solution (caution, fumes). Next, the

terephthalic acid was added to the solution and again sonicated to dissolve. Finally, water was added, the solution was stirred, placed into a glass pressure vessel, sealed, and heated in a pre-heated oven at 120 °C for 21 hours. Following synthesis, the powdery white product was recovered by vacuum filtration and washed with DMF, ethanol, and acetone. To ensure complete exchange of pore solvent/impurities with water, the samples were soaked in acetone (3 x 20 mL) followed by ultra-high-purity water (3 x 20 mL) for one day each in a centrifuge tube and were recovered each time by centrifugation. Finally, the samples were dried in an oven at ~60°C for 24 hours.

We found that the synthesis of this material relied heavily upon the water content present, particularly if fresh DMF and ZrCl₄ were used for synthesis. With insufficient water present, we would obtain either an amorphous phase or a poorly crystalline MIL-140A (ZrO(C₈H₄O₄)) phase.³ With too much water, we would obtain an amorphous byproduct co-phase, particularly with non-molar equivalents of Zr: terephthalate. The presence of this secondary phase was confirmed with TEM (Figure S2, d).

Table S1. Amounts of reagents used for the synthesis of samples 1 – 6.

Sample #	ZrCl ₄ (mmol)	Terephthalic acid (mmol)	Acetic acid (mmol)	Stearic acid (mmol)	Water (mmol)	DMF (mL)
1	3.60	3.88	-	-	11.1	67.5
2	2.66	1.75	-	-	5.0	60.0
3	2.66	1.35	-	-	5.9	60.0
4	3.43	3.49	3.5	-	11.1	60.0
5	3.66	4.12	-	2.06	11.1	60.0
6	3.66	4.12	-	17.6	11.1	60.0

Defect Quantification. Thermogravimetric analysis was performed using a Bruker AXS TGA-DTA 2000-SA in aluminium pans under air from 20 °C to 550 °C at a rate of 2 °C/min. Samples **1 – 3, 5** and **6** showed three mass loss steps, with water solvent loss from room temperature to ~130 °C, dehydration of the zirconium cluster from ~200 – 300 °C, followed by an exothermic decomposition from ~380 – 500 °C to form ZrO₂. Defect formulae were calculated by analysing the mass loss in the decomposition step progressing from a formula of Zr₆O_{6+x}(C₈H₄O₄)_{6-x} at 300 °C to 6·ZrO₂ at 550 °C with an expected UiO-66/6·ZrO₂ ratio of 2.20 for x = 0. The x values for samples were 0.3 for **1**, 0.8 for **2**, and 1.4 for **3**, 0.4 for **5** and 1.0 for **6** (Figure S1). EA was also used to quantify the defects using a formula of Zr₆O_{6+x}(C₈H₄O₄)_{6-x}·yH₂O and equating to the values found by TGA. Samples were evacuated at 180 °C under vacuum and subsequently back-filled with dry N₂ prior to EA but were exposed to air briefly before analysis. The values of x and y for the samples were 0.3 and 2.3 for **1** (calc. 1.70% H, 33.70% C, found 1.99% H, 33.70% C), 0.8 and 2.2 for **2** (calc. 1.64% H, 32.25% C, found 1.93% H, 32.48% C), 1.4 and 2.7 for **3** (calc. 1.63% H, 30.08% C, found 1.85% H, 30.34% C), 0.4 and 7.2 for **5** (calc. 2.18% H, 31.68% C, found 2.22% H, 31.64% C), and 1.0 and 10.5 for **6** (calc. 2.47% H, 28.78% C, found 2.41% H, 28.66% C). For sample **4**, the defect amount was determined using a formula of Zr₆O₆(C₈H₄O₄)_{6-x}(O₂C₂H₃)_{2x}·yH₂O. To simplify the TG analysis, **4** was activated at 350°C for 48 hours to completely remove the acetate ligands (confirmed by ¹³C CP-MAS NMR), and TG analysis was performed; x = 0.7 was found from TGA. EA was performed on the sample **4** after activation at 180°C (no acetate removal) with x and y values of 0.7 and 3 found (calc. 1.91% H, 32.90% C, found 1.95% H, 32.88% C). To determine whether acetate or stearate remained in samples **4 – 6**, the samples (~20 mg) were placed in D₂O solution

(~0.5 mL) to which NH_4F was added until the solution became clear and colourless. $^1\text{H-NMR}$ was performed using a 600 MHz JEOL JNM-ECA 600 NMR spectrometer. Sample **4** had two peaks at 8.10 ppm (s) (terephthalate aromatic -H) and 2.15 ppm (s) (acetate $-\text{CH}_3$), whereas samples **5** and **6** had a one peak at 8.10 ppm (s).

Powder X-ray diffraction. Powder X-ray diffraction (PXRD) was carried out on a Bruker D8 Advance instrument equipped with a $\text{CuK}\alpha$ X-ray source ($\lambda = 1.54059 \text{ \AA}$) from 5° to $60^\circ 2\theta$. Samples were visually compared with a simulated pattern of UiO-66 with no apparent erroneous peaks.

Sorption analysis. Gas and vapour sorption analysis was performed using a BEL Japan BELSORP-Max instrument using N_2 gas (99.999%) at 77 K with a liquid nitrogen bath or using H_2O (double deionized, distilled, and degassed) at 298 K with a circulating ethylene glycol bath to maintain constant temperature. Samples were thoroughly activated prior to sorption analysis under vacuum at 150°C for 24 hours. Adsorption and desorption cycles were performed for all analyses.

Transmission electron microscopy. Transmission electron microscopy (TEM) was performed using a Hitachi HT7700 TEM operated at 100 kV.

Impedance analysis. Proton conductivity testing was carried out on pelletized samples pressed in a cylindrical die (2.5 mm diameter, 0.8-1.2 mm length) at ~0.3 GPa for only 30 seconds to prevent sample decomposition from the high pressure. Electrodes were affixed to the pellets using gold paste, and the samples were held between spring-loaded flat titanium plates to prevent electrode delamination. Impedance analysis was performed on the pellets using a quasi-four-probe method with a Solartron 1260 Impedance/Gain-Phase Analyzer from 10 MHz – 1 Hz.

For high impedance samples ($> 10^6 \Omega$), a two probe method using a Solartron 1260 Impedance/Gain-Phase Analyzer fitted with a Solartron 1296 Dielectric Interface was used, and data were collected from 1 MHz – 1 Hz. Humidity and temperature were controlled using an Espec SH-221 humidity control chamber. Multiple scans were performed under a given set of conditions until the Nyquist plots overlaid, showing that the sample had reached equilibrium (typically 3-5 hours for equilibration). The resistance value was determined from equivalent circuit fits of the first semi-circle using Zplot software. Activation energy for proton transport was calculated from the variable temperature data at constant relative humidity after two heating/cooling cycles using the Arrhenius equation $\sigma = (\sigma_0/T)\exp(-E_a/kT)$, where σ is conductivity, σ_0 is a pre-exponential factor, T is temperature, k is the Boltzmann constant, and E_a is the activation energy.

^{13}C Cross Polarisation Magic Angle Spinning Nuclear Magnetic Resonance

Spectroscopy. ^{13}C CP-MAS NMR spectroscopy was performed at room temperature using a Bruker Biospin K.K., ADVANCE II⁺ 400 NMR spectrometer at a frequency of 100.6 MHz and a spinning rate of 10 kHz at the magic angle. Measurements were performed at room temperature on hydrated samples of **4** before and after activation at 350°C as well as on hydrated sample **3**. Sample **3** and **4** after activation showed three peaks corresponding to the asymmetric unit of UiO-66, with chemical shifts of 171.7 ppm ($\text{O}_2\text{C-R}$), 137.2 ppm (aromatic C), and a broader peak at 129.1 ppm (aromatic C-H). Sample **4** before activation showed two extra peaks corresponding to the acetate groups at 176.4 ppm (acetate $\text{O}_2\text{C-R}$) and 24.0 ppm (acetate R-CH_3) together with the terephthalate signals at 171.7 ppm (terephthalate $\text{O}_2\text{C-R}$), and 137.2 ppm (aromatic C). Interestingly, the aromatic C-H signal in this sample split into two signals at 130.8 ppm and 128.4 ppm.

Pulsed-Field Gradient Nuclear Magnetic Resonance Spectroscopy. ¹H PFG-NMR

spectroscopy was performed using a Bruker Biospin K.K., ADVANCE II⁺ 400 NMR spectrometer at a frequency of 400 MHz equipped with a Bruker Biospin K.K. Diff 50 diffusion probe. Temperature calibration was performed using ethylene glycol prior to the measurement. Solid samples of **3** or **6** were first loaded into an NMR tube and were then mixed with 1 drop of ultrapure water, sealed, and equilibrated at 65 °C in an oven for 2 hours prior to measurement. Measurements were collected at 338.2 K using stimulated echo experiments (Figure S11) at 16 gradient field strengths, and the diffusion coefficient was calculated using the Stejskal-Tanner equation:^{4,5}

$$\frac{S}{S_0} = e^{-\gamma^2 g^2 \delta^2 \left(\Delta - \frac{\delta}{3}\right) D}$$

Where S is the signal intensity, S_0 is the signal intensity at zero gradient field, γ is the gyromagnetic ratio of the proton, g is the gradient field strength, δ is the effective gradient pulse duration, Δ is the diffusion time and D is the diffusion coefficient. The parameters used for the experiments are given in Table S3. With increasing gradient field strength, two sharp signals were observed at -3.00 ppm and -5.48 ppm, with the signal at -3.00 ppm decaying rapidly as g was increased, and the signal at -5.48 ppm decaying more slowly with increasing g . The signal at -3.00 ppm was determined to be bulk water as the signal intensity increased significantly by the addition of excess water to the sample. If the sample was measured at lower relative humidity (less than ~20% RH at 65 °C), neither of the signals could be observed in the spectra, meaning both were derived from water. Representative spectra are shown in figure S9 and the linearized intensity data is given in figure S10.

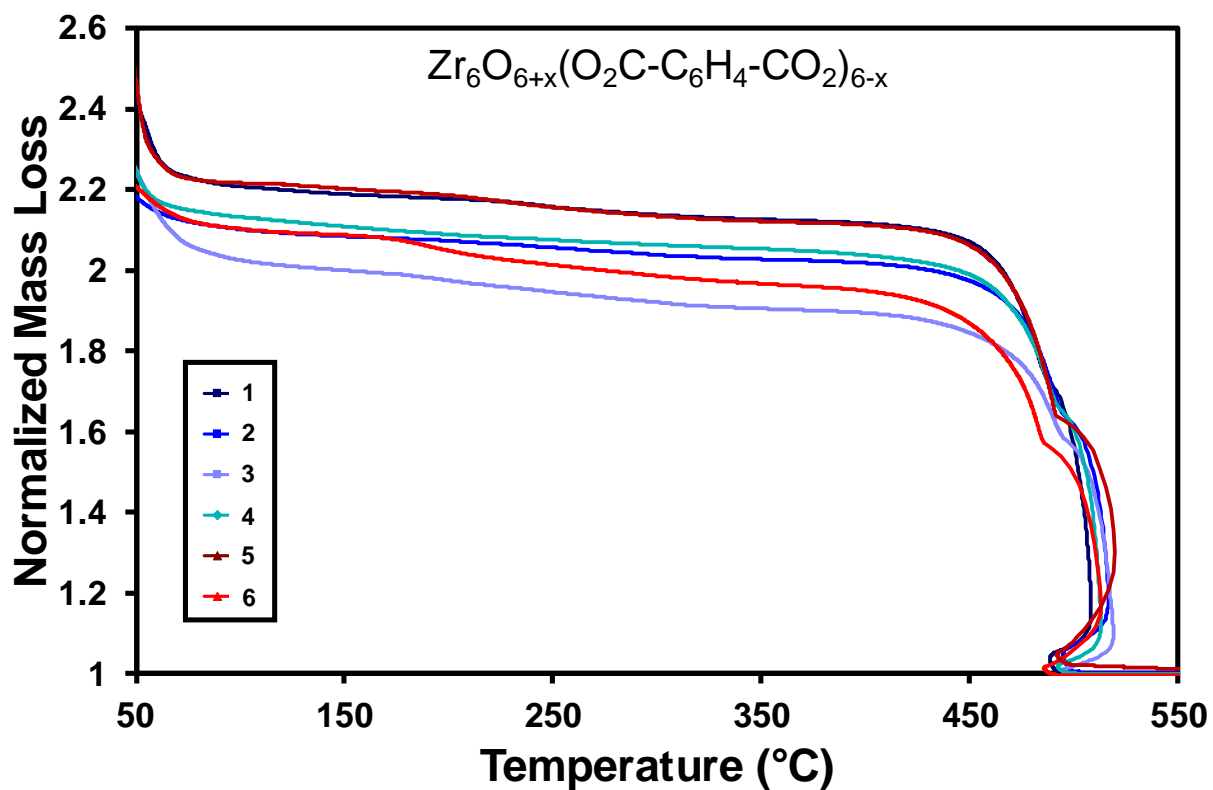


Figure S1. Normalized TGA thermal curves for samples **1 – 6** collected under air flow, normalized to the mass of the ZrO_2 decomposition product. Sample 4 was activated at $350\text{ }^\circ\text{C}$ for 48 hrs prior to analysis to remove acetate. A normalized mass loss of 2.2 corresponds to a defect free sample ($x = 0$).

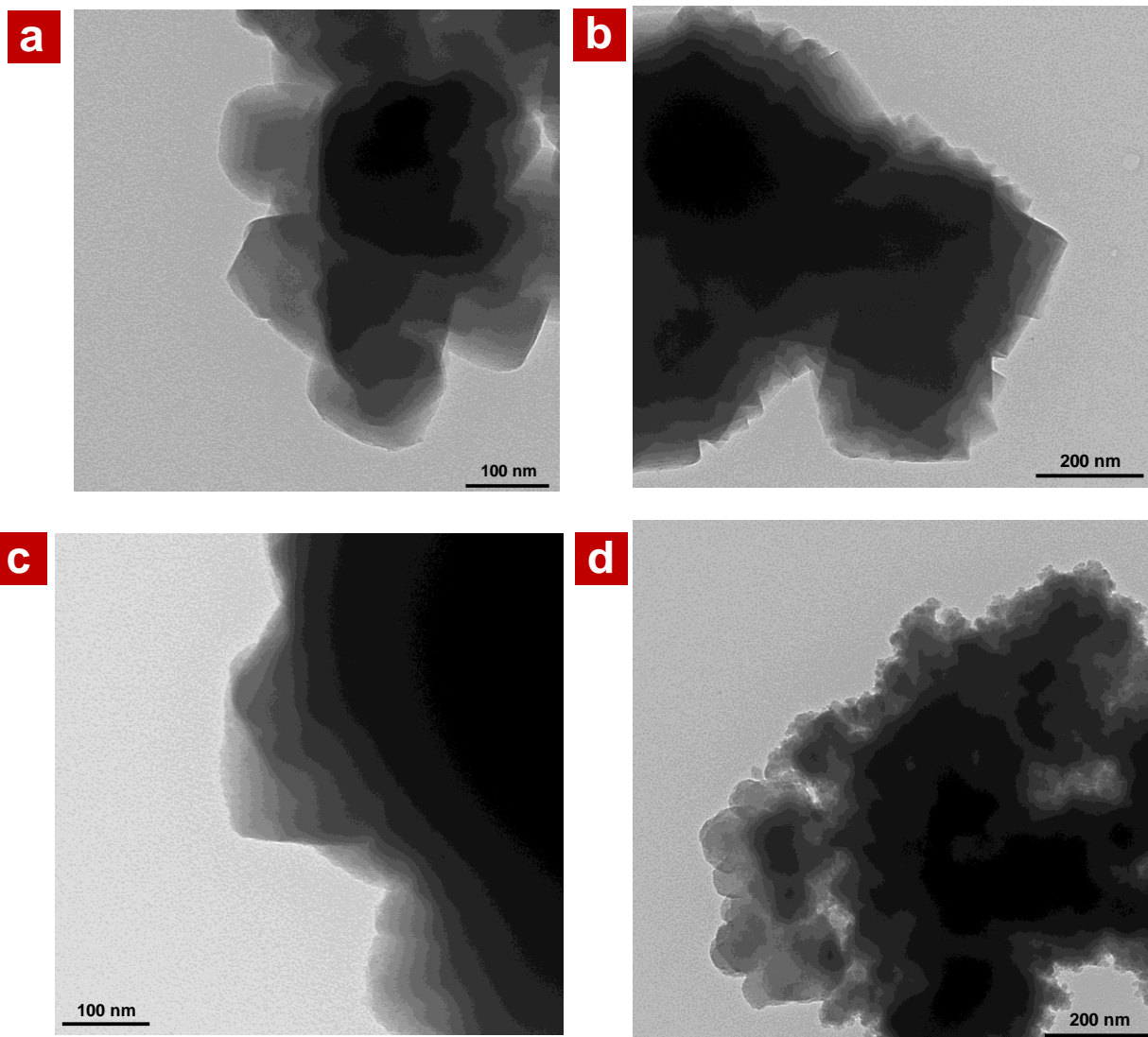


Figure S2. Representative TEM images from samples. Samples **1** (a), **2** (b), **3** (c), and a sample synthesized with less than 0.5 terephthalic acid to ZrCl_4 ratio (d). Note the mixture of large and small particles in (d).

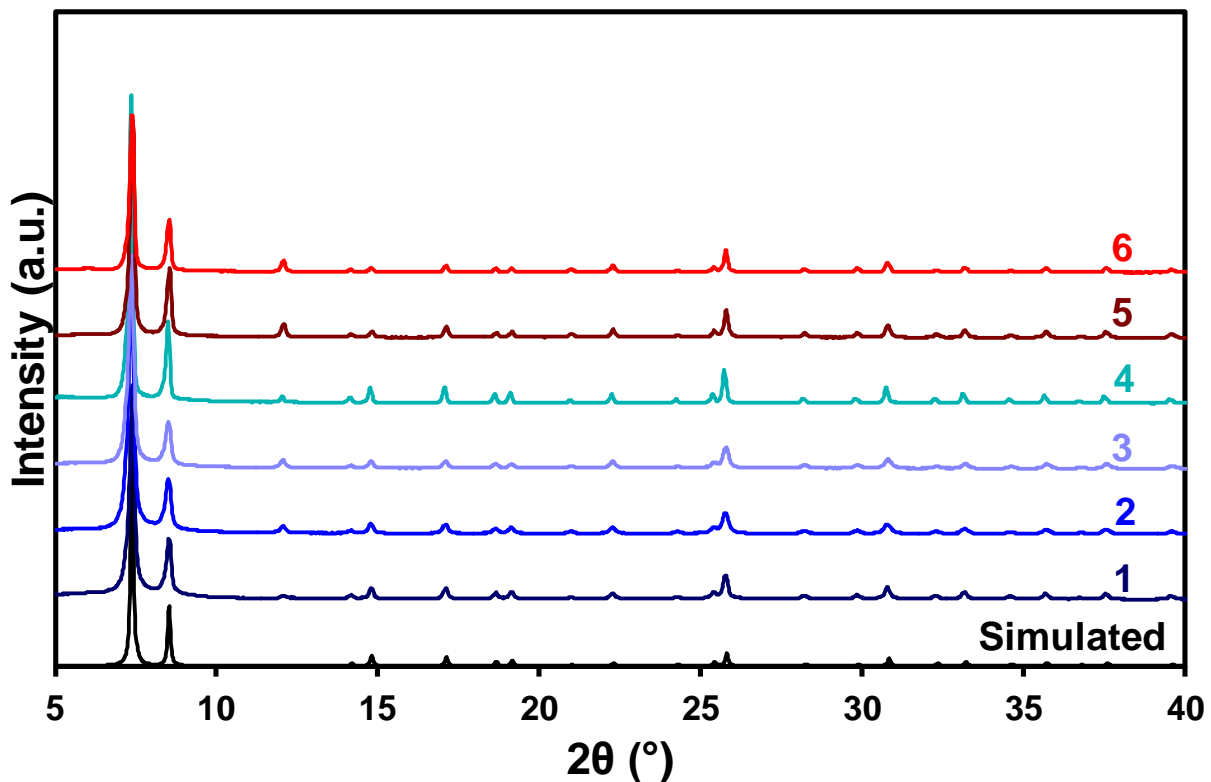


Figure S3. PXRD patterns of samples **1** – **6** after washing procedures but before impedance analysis. The simulated pattern of UiO-66 (black) is given at the bottom of the chart.

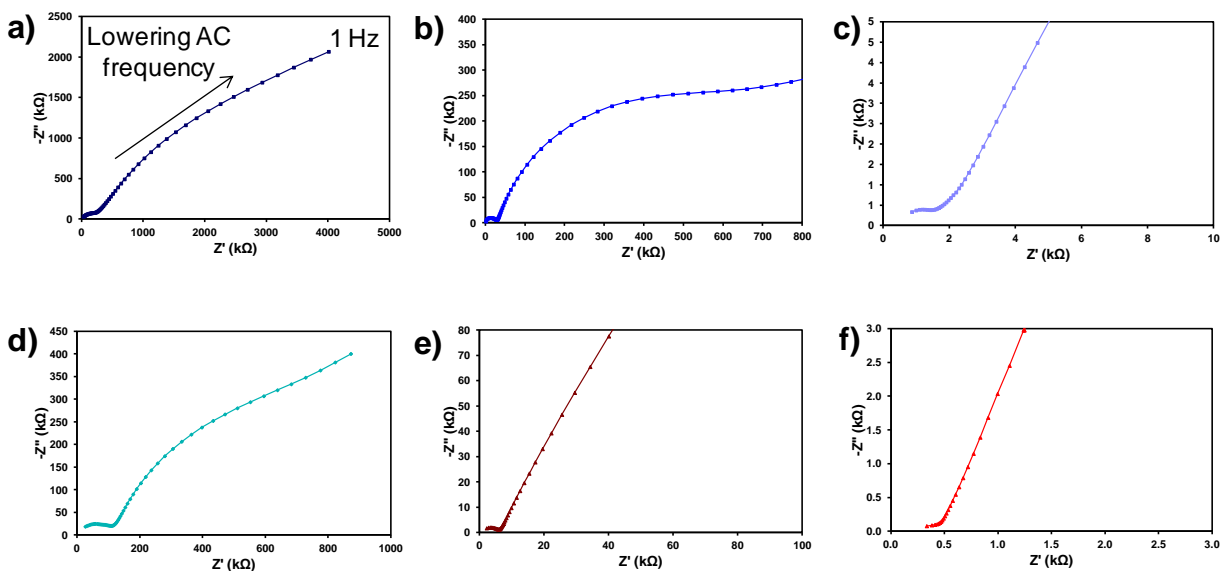


Figure S4. Representative Nyquist plots for samples **1** – **6**. **1** (a), **2** (b), **3** (c), **4** (d), **5** (e) and **6** (f) were all collected after equilibration at 65 °C and 95%RH. Samples **1** and **4** were collected from 1 MHz to 1 Hz, while samples **2**, **3**, **5** and **6** were collected from 10 MHz to 1 Hz.

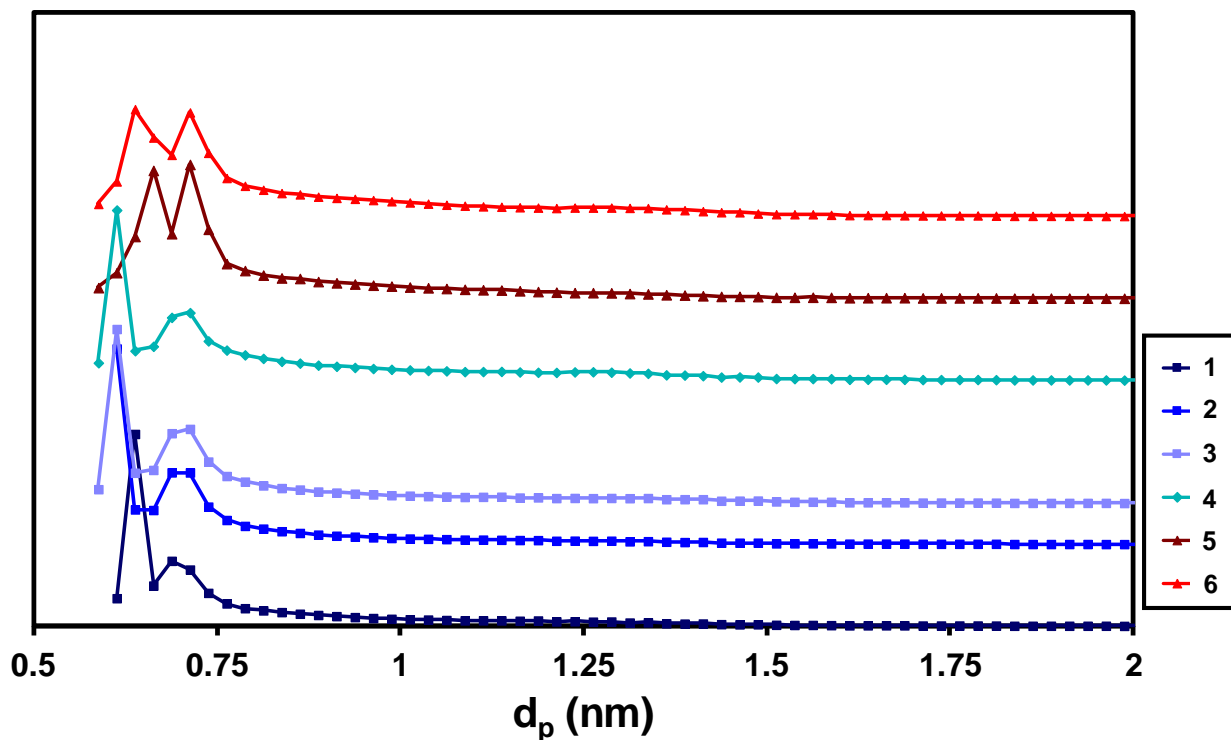


Figure S5. Horvath-Kawazoe micropore size distribution for samples 1 – 6.

Table S2. Micropore volume calculated using Horvath-Kawazoe micropore analysis for samples 1 – 6.

	1	2	3	4	5	6
First peak pore volume (cm³/g)	0.149	0.153	0.125	0.125	0.161	0.165
Second peak pore volume (cm³/g)	0.127	0.142	0.168	0.161	0.190	0.155
larger pores volume (cm³/g)	0.142	0.119	0.157	0.205	0.180	0.253
First and second peak combined volume (cm³/g)	0.276	0.296	0.293	0.286	0.351	0.320
Total micropore volume (cm³/g)	0.418	0.414	0.450	0.491	0.531	0.574

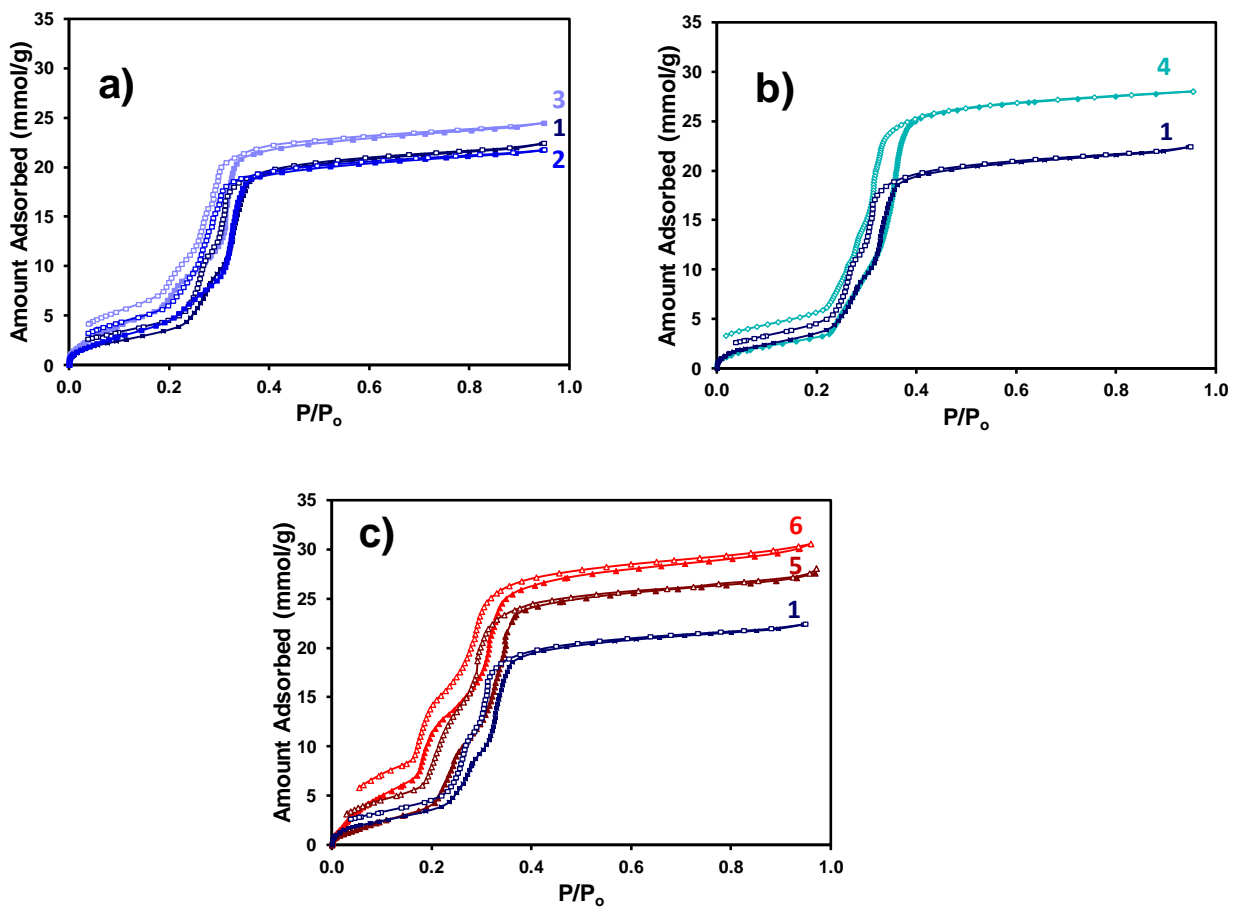


Figure S6. Water vapour sorption analysis of samples **1 – 3** (a), **1 and 4** (b), and **1, 5 and 6** (c) at 298 K with desorption isotherms included. Adsorption isotherms are filled shapes while desorption isotherms are unfilled.

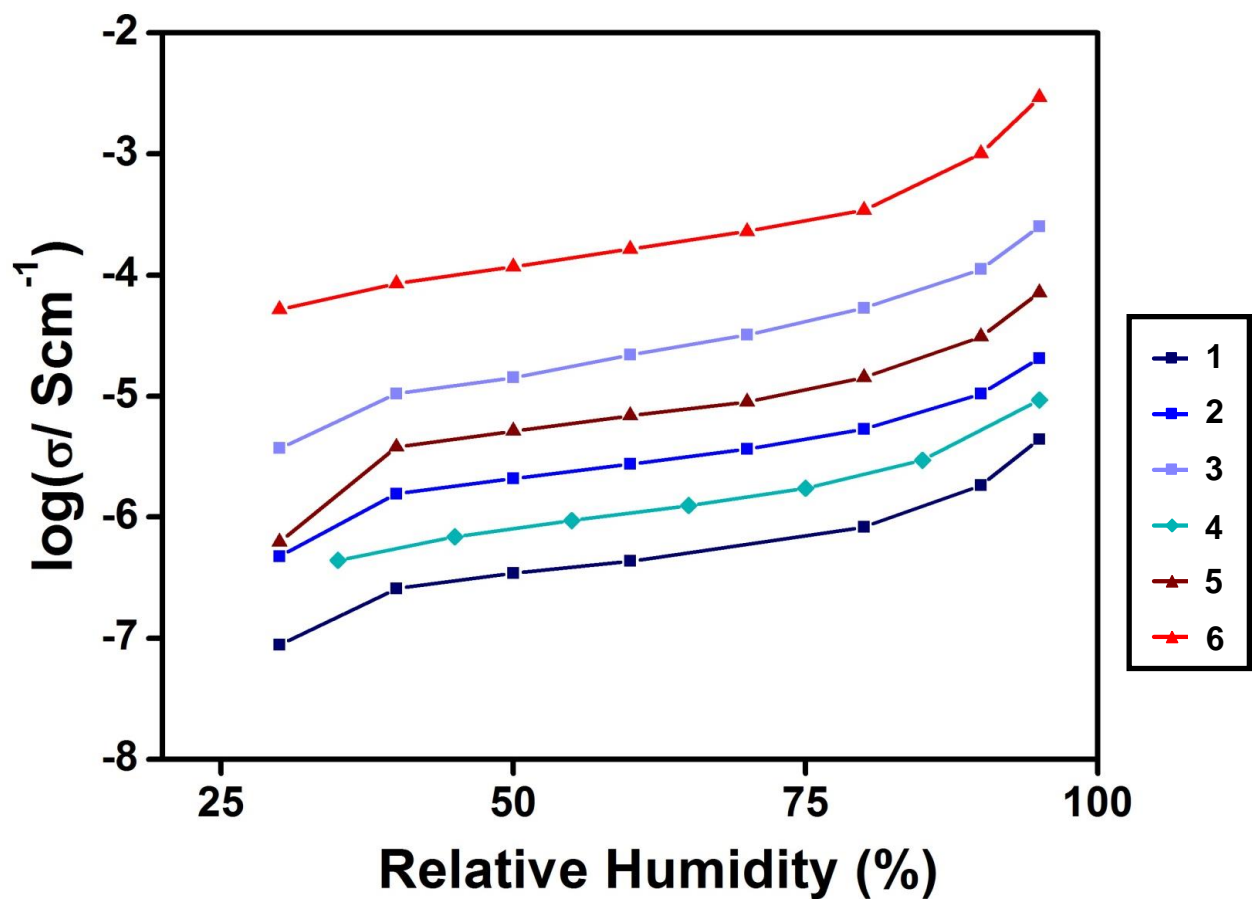


Figure S7. Variable humidity impedance analysis of samples 1 – 6 collected at 25 °C.

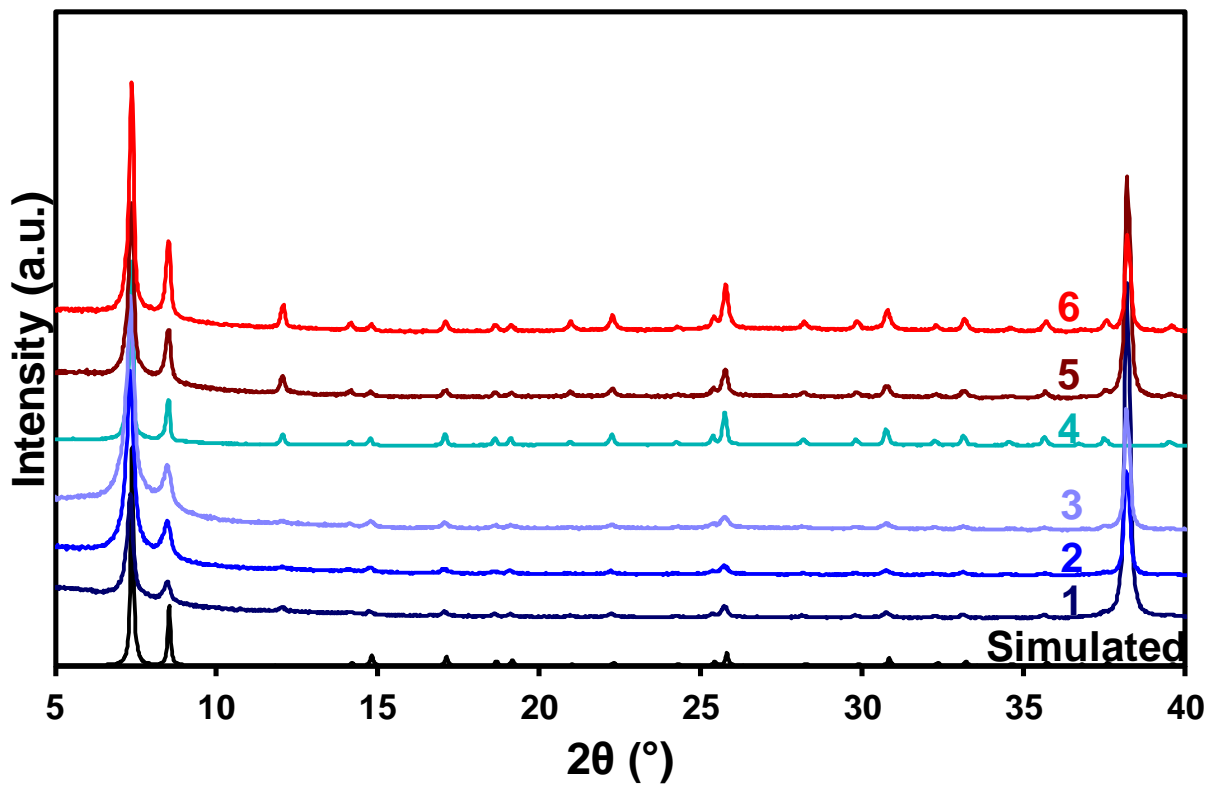


Figure S8. PXRD patterns of samples **1** – **4** after pelletization and impedance analysis. The reduction in intensity is partially due to the small amount of sample used for impedance analysis (~4 mg). The peak at 38.2° 2θ results from the gold electrode that was affixed to the pellets.

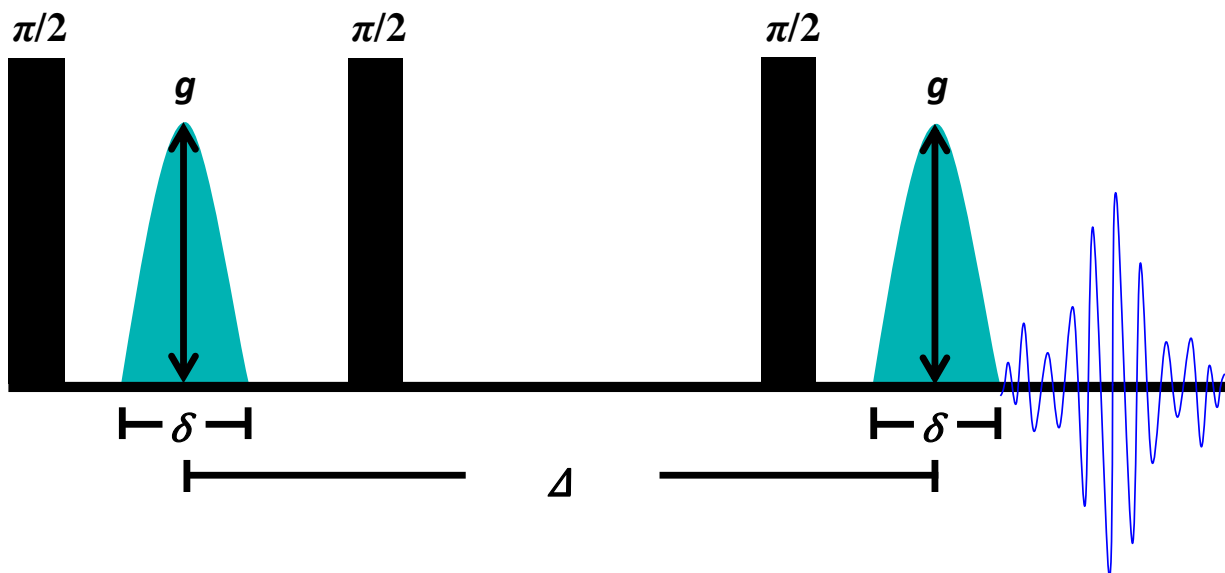


Figure S9. Pulsed gradient stimulated echo sequence used for the PFG-NMR analysis, where g is the gradient field strength, δ is the effective gradient pulse duration, Δ is the diffusion time.

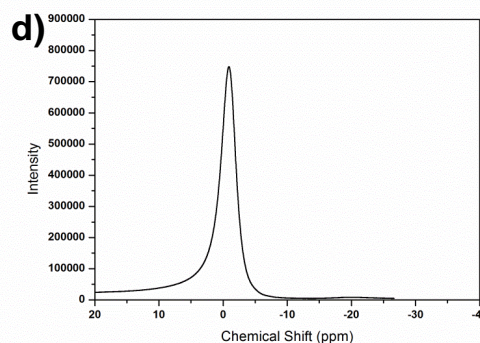
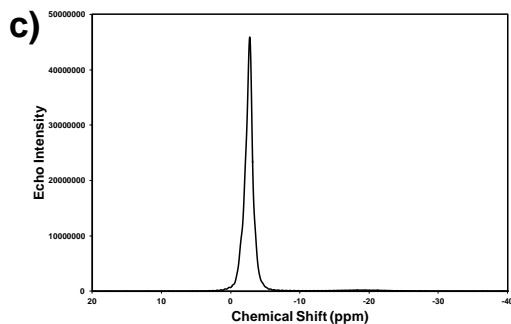
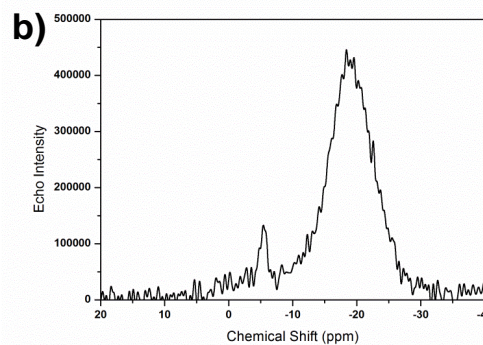
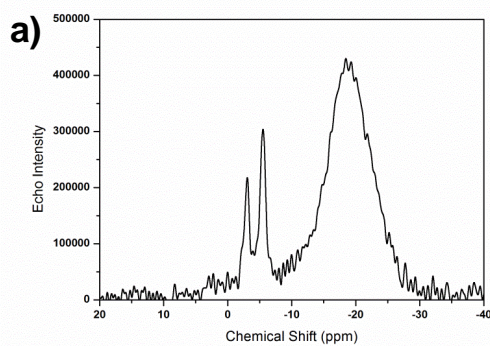


Figure S10. Representative PFG-NMR spectra from sample **6**, with stimulated echo at low gradient (a), high gradient (b), and with an excess water added to the sample at low gradient (c). The spectrum from a single 90° pulse is also shown (d).

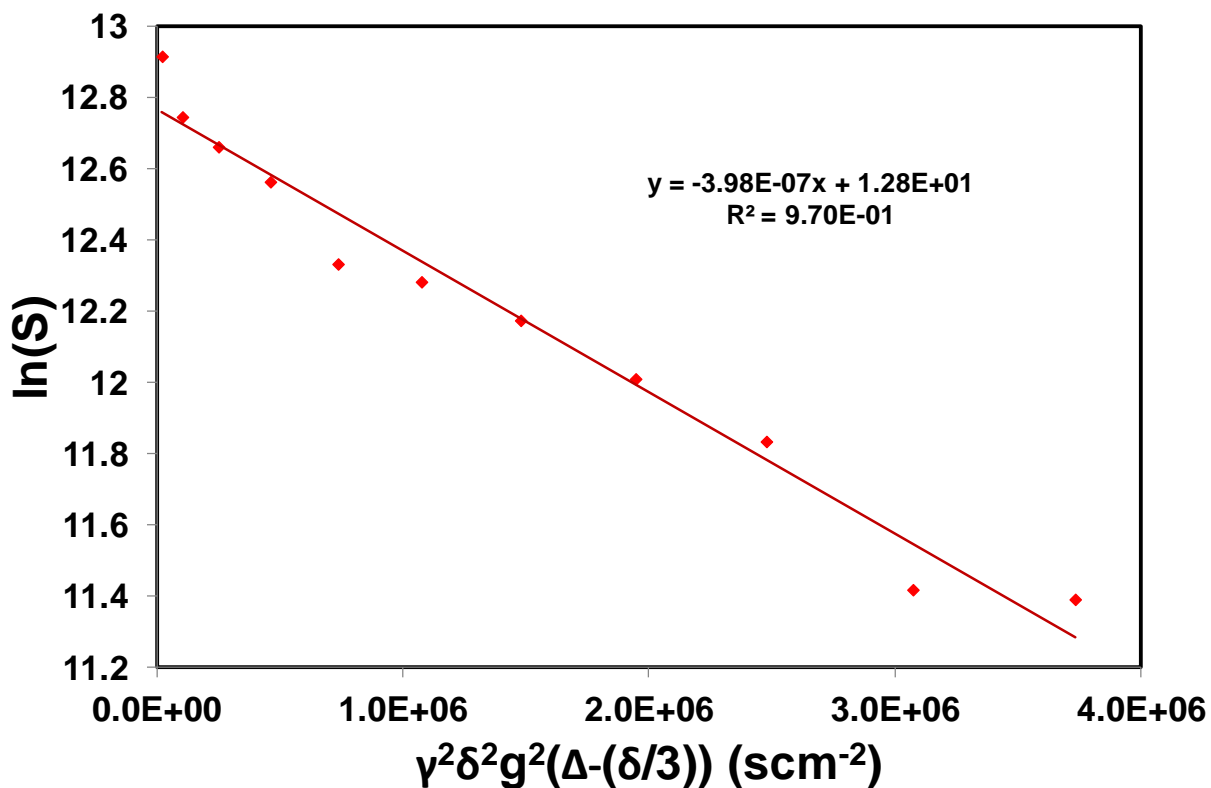


Figure S11. The natural logarithm of echo signal intensity ($\ln(S)$) versus $\gamma^2\delta^2g^2(\Delta-(\delta/3))$ for sample **6**, where γ is the gyromagnetic ratio of a proton, δ is the effective gradient pulse duration, and Δ is the diffusion time. The apparent diffusion coefficient in cm^2s^{-1} is the absolute value of the slope (line equation inset).

Table S3. PFG-NMR experimental parameters.

Sample #	Δ (ms)	δ (ms)	Starting g (G/cm)	Maximum g (G/cm)	Number of gradient steps
2	40.00	1.00	124.90	2497.90	16
6	20.00	0.50	74.93	1501.05	16

References.

- (1) Cavka, J. H.; Jakobsen, S.; Olsbye, U.; Guillou, N.; Lamberti, C.; Bordiga, S.; Lillerud, K. P. *J. Am. Chem. Soc.* **2008**, *130*, 13850.
- (2) Schaate, A.; Roy, P.; Godt, A.; Lippke, J.; Waltz, F.; Wiebcke, M.; Behrens, P. *Chem. Eur. J.* **2011**, *17*, 6643.

- (3) Guillerm, V.; Ragon, F.; Dan-Hardi, M.; Devic, T.; Vishnuvarthan, M.; Campo, B.; Vimont, A.; Clet, G.; Yang, Q.; Maurin, G.; Férey, G.; Vittadini, A.; Gross, S.; Serre, C. *Angew. Chem. Int. Ed.* **2012**, *51*, 9267.
- (4) Stejskal, E. O.; Tanner, J. E. *J. Chem. Phys.* **1965**, *42*, 288.
- (5) Tanner, J. E. *J. Chem. Phys.* **1970**, *52*, 2523.